



Fe–C micro-alloying effect on properties of $Zr_{53}Al_{11.6}Ni_{11.7}Cu_{23.7}$ bulk metallic glass

Da-wei DING^{1,2}, JING TAN³, An-hui CAI³, Yong LIU⁴,
Hong WU⁴, Qi AN³, Peng-wei LI³, Yan ZHANG³, Qing YANG³

1. Institute of Physics, Chinese Academy of Sciences, Beijing 100190, China;

2. Songshan Lake Materials Laboratory, Dongguan 523808, China;

3. College of Mechanical Engineering, Hunan Institute of Science and Technology, Yueyang 414000, China;

4. State Key Laboratory of Powder Metallurgy, Central South University, Changsha 410083, China

Received 19 September 2020; accepted 3 March 2021

Abstract: $(Zr_{53}Al_{11.6}Ni_{11.7}Cu_{23.7})_{1-x}(Fe_{77.1}C_{22.9})_x$ ($x=0-2.2$, at.%) bulk metallic glasses (BMGs) were prepared by copper mold suction casting method. Their glass forming ability and physical and chemical properties were systematically investigated. The glass forming ability is firstly improved with increasing x , and then decreased when x exceeds 0.44 at.%. Both glass transition temperature and crystallization temperature are increased, while the supercooled liquid region is narrowed, with Fe–C micro-alloying. The hardness, yielding and fracture strength, and plasticity firstly increase and then decrease when x reaches up to 1.32 at.%. The plasticity of the BMG ($x=1.32$ at.%) is six times that of the Fe-free and C-free BMG. In addition, by the Fe–C micro-alloying, the corrosion potential is slightly decreased, while the corrosion current density increases. The pitting corrosion becomes increasingly serious with the increase of Fe and C content.

Key words: Zr-based metallic glass; corrosion property; thermal property; mechanical property; Fe–C micro-alloying

1 Introduction

Zr-based metallic glasses (MGs) have been thought to be the promising structural and functional materials due to their excellent chemical and physical properties [1], such as good glass forming ability (GFA) and wide supercooled liquid region [1], good wear- or corrosion-resistance [2–4], good bio-compatibility [3–8] and antibacterial activity [9–12], excellent near-infrared transmission [13], and good oil/water separation capacity [14]. However, room-temperature embrittlement of the MGs is fatal for their practical engineering applications, although some Zr-based BMGs with good room-temperature plasticity [6–8,15,16] have been successfully developed. In addition, increasing

researches have declared that there are contradictory relationships among the properties of the MGs/bulk metallic glasses (BMGs), such as size-dependent plasticity [17–19]. Yet, some Zr-based MGs with the combination of high GFA and good properties have been developed by adjusting the alloy compositions [4–7]. Thus, it is a challenging and interesting issue for developing the MGs with high comprehensive properties in order to satisfy the increasingly stringent requirements.

Microalloying or minor addition has been confirmed as one of effective strategies for combinatorially improving the properties of the MGs/BMGs. The usual addition elements for Zr-based MGs include Ag [4,20–23], Ta [24,25], Nb [26–28], Hf [29], Ti [30–33], Al [4,34,35], Y [36–40], Co [41–46], Lu [47], Pd [48], Sn [49],

Si [35,50,51], Ca [52], V [53], Cu [54], etc. For instance, CUI et al [23] found that the substitution of Ti with Ag can significantly improve both the GFA and mechanical properties of $Zr_{57}Cu_{20}Al_{10}Ni_8Ti_{5-x}Ag_x$ ($x=0-5$ at.%) BMGs. JIN et al [29] prepared a series of $Zr_{55}Ti_3Hf_xCu_{32-x}Al_{10}$ ($x=0-5$ at.%) BMGs by copper mold suction-casting, and found that the GFA, supercooled liquid region, compressive yield strength, room-temperature plasticity and corrosion resistance are simultaneously improved by Hf addition. In addition, Fe [55–60] and C [61–64] elements are also considered as the effective additives for enhancing the GFA and the properties of Zr-based MGs/BMGs due to their smaller atomic radii. For example, LIU et al [58] found that Fe addition can increase the glass transition temperature, crystallization temperature, compressive fracture strength and plasticity, but decrease the supercooled liquid region of $(Zr_{0.55}Al_{0.10}Ni_{0.05}Cu_{0.30})_{100-x}Fe_x$ ($x=0-4$ at.%) alloys. ZHOU et al [59] found that Fe addition can remarkably enhance the glass transition temperature, crystallization temperature, supercooled liquid region, plastic strain as well as the GFA of $Zr_{65}Cu_{17.5}Al_{7.5}Ni_{10-x}Fe_x$ ($x=0-10$ at.%) alloys. On the other hand, It was found that C addition deteriorated the GFA [61,62] but enhanced the thermal stability and microhardness [61] of $Zr_{41}Ti_{14}Cu_{12.5}Ni_{10}Be_{22.5}$ alloy. KÜNDIG et al [63] found that the GFA of $Zr_{52.5}Cu_{17.9}Ni_{14.6}Al_{10}Ti_5$ alloy increased and then decreased when the C content exceeds 0.1 at.%. WANG et al [64] investigated the effect of C addition on the microstructure and properties of laser cladding $(Zr_{65}Al_{7.5}Ni_{10}Cu_{17.5})_{100-x}C_x$ ($x=0, 3, 5$ and 10) coatings. They found that C addition can improve the microhardness and lower the friction coefficient of the amorphous composite coating.

As mentioned above, the influence of Fe addition on the GFA and thermal and mechanical properties of Zr-based alloys depended on Fe content and alloy compositions. In addition, the effect of Fe addition on other properties such as corrosion resistance of Zr-based alloys has less been investigated. Compared with the Fe addition, the effect of C addition on the GFA and the properties of Zr-based alloys has been investigated more inadequately. To our best knowledge, the synergistic effects of Fe and C additions on both GFA and properties of Zr-based BMGs have not

been reported. In the present work, a series of Zr–Al–Ni–Cu–Fe–C BMGs were prepared by copper mold suction casting method. The Fe–C micro-alloying effect on thermal, mechanical and corrosive properties as well as glass forming ability of $Zr_{53}Al_{11.6}Ni_{11.7}Cu_{23.7}$ alloy was systematically investigated.

2 Experimental

The $(Zr_{53}Al_{11.6}Ni_{11.7}Cu_{23.7})_{1-x}(Fe_{77.1}C_{22.9})_x$ ($x=0-2.2$ at.%) alloy ingots were prepared by mixing high purity raw materials through arc melting method in a high purity argon atmosphere. The ingots were flipped and remelted at least four times to ensure their composition uniformity. The purity of the raw materials for Zr, Al, Ni and Cu is 99.99 wt%. Fe and C were added as Fe–C alloy containing 6 wt.% C, whose purity is 99.99 wt.%. The alloy rods with 2 mm in diameter were obtained by suction casting method. The amorphous structure of these as-cast samples was examined by XD-3A diffractometer with $Cu K_{\alpha}$. The crystallization characteristics were investigated by a DSC-3 differential scanning calorimeter (DSC) at heating rate of 40 K/min under high purity flowing nitrogen. DSC-404C differential scanning calorimeter was applied to characterizing the melting nature under high purity flowing argon at heating rate of 40 K/min. Uniaxial room-temperature compression measurements were conducted on the Zr-based BMGs with 2:1 aspect ratio by an Instron 3369 testing machine at loading rate of $1 \times 10^{-5} s^{-1}$. Two ends of the compression specimens were mirror-polished to be parallel to each other and perpendicular to its radial direction. The hardness was measured by HR-150A Rockwell hardness tester under a load of 150 kg for 30 s. The corrosion behavior was evaluated by electrochemical polarization test at sweep rate of 0.001 V/s from -2.0 to 4.5 V in 2 wt.% hydrochloric acid solution. Electrochemical tests were performed by three-electrode method and operated after the stable open-circuit potential was reached. The counter electrode and the reference electrode are platinum and saturated calomel electrode (SCE), respectively. The measured surfaces (~ 3 mm²) as the working electrode were mirror-polished and the rest of the specimen was embedded in a thermoplastic resin to ensure

electrical isolation. Microstructure of fracture and corrosion specimens was analyzed using SIRION scanning electron microscopy (SEM) operated at 30 kV. The chemical compositions of the corroded surfaces were analyzed using Buehler energy dispersive spectrometer (EDS) equipped with the SEM.

3 Results

Figure 1 shows XRD patterns for the studied Zr-based glass forming alloys. One can clearly observe from Fig. 1 that there is a broad diffraction hump in the 2θ range of 30° – 50° characterized in the amorphous state and no sharp crystal diffraction peaks for each glass forming alloy. It is indicated that the as-cast Zr-based glass forming alloys are all in amorphous structure.

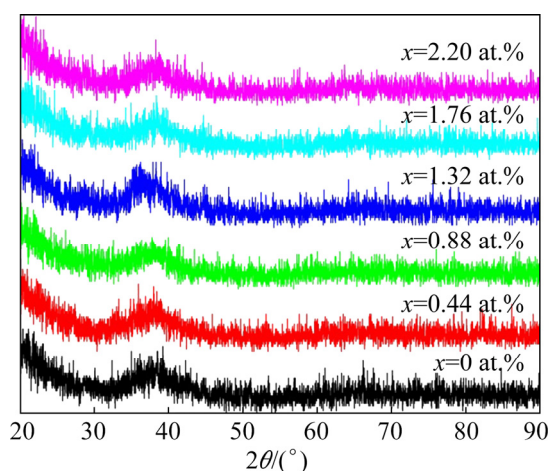


Fig. 1 XRD patterns of $(Zr_{53}Al_{11.6}Ni_{11.7}Cu_{23.7})_{1-x}-(Fe_{77.1}C_{22.9})_x$ ($x=0-2.2$) glass forming alloys

DSC measurements were conducted at a heating rate of 40 K/min and the typical DSC traces are presented in Fig. 2(a). It can be seen from Fig. 2(a) that there is an endothermic peak for the glass transition and an exothermic peak for the crystallization for each alloy. This implies that all studied Zr-based BMGs are in amorphous feature owing to the glass transition process and characterize in one-step crystallization behavior for one crystallization procedure. In addition, glass transition temperature T_g , onset crystallization temperature T_x , and supercooled liquid region ΔT_x are thoroughly determined and tabulated in Table 1. As seen, both T_g and T_x are increased by the Fe and C additions, which is similar to the effect of Fe

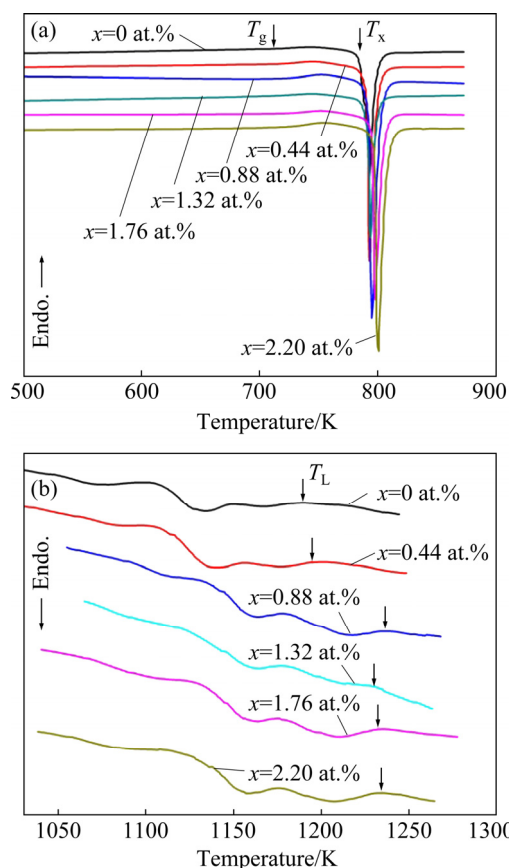


Fig. 2 DSC (a) and DTA (b) curves of $(Zr_{53}Al_{11.6}Ni_{11.7}Cu_{23.7})_{1-x}-(Fe_{77.1}C_{22.9})_x$ ($x=0-2.2$) at heating rate of 40 K/min

addition on $Zr_{55}Al_{10}Ni_5Cu_{30}$ alloy [58] and the effect of C addition on $Zr_{41}Ti_{14}Cu_{12.5}Ni_{10}Be_{22.5}$ alloy [61]. However, the ΔT_x is narrowed by the Fe and C additions, which is opposite to the results in Refs. [59,61] and similar to the results in Refs. [55,58]. The increase of T_g and T_x indicates that both glass transition and crystallization are retarded. The thermal stability is deteriorated due to the narrowed ΔT_x . On the other hand, the melting features were studied by DTA at a heating rate of 40 K/min. The typical DTA curves are shown in Fig. 2(b). Three endothermic peaks corresponding to the melting procedures can be obviously observed from Fig. 2(b). Three melting stages and the liquidus temperature T_L are shifted towards high temperature by Fe and C additions. High Fe and C contents are more effective for the rise of T_L . These results are similar to the results in Refs. [56,58] and on the contrary to the results in Refs. [57,59,62]. Moreover, glass forming ability (GFA) of the studied Zr-based BMGs was estimated by a well-known indicator of reduced glass transition

Table 1 Glass transition temperature T_g , onset crystallization temperature T_x , supercooled liquid region ΔT_x , liquidus temperature T_L , reduced glass transition temperature $T_{rg}(=T_g/T_L)$, hardness, yield strength σ_y , fracture strength σ_f , plastic strain ε_p , corrosion current density J_c , and corrosion potential φ_c for $(Zr_{53}Al_{11.6}Ni_{11.7}Cu_{23.7})_{1-x}(Fe_{77.1}C_{22.9})_x$ ($x=0-2.2$) bulk metallic glasses

x /at.%	T_g /K	T_x /K	ΔT_x /K	T_L /K	T_{rg}	Hardness (HRC)	σ_y /MPa	σ_f /MPa	ε_p /%	J_c /(A·cm ⁻²)	φ_c /V
0	712.7	791.2	78.5	1191.7	0.598	47.0	1667.1	1778.0	0.3	9.82×10^{-6}	-0.24
0.44	720.0	792.6	72.6	1194.1	0.603	49.0	1751.1	1892.0	0.4	2.98×10^{-5}	-0.26
0.88	724.1	792.8	68.7	1238.4	0.585	50.0	1762.0	2030.9	0.8	1.27×10^{-4}	-0.26
1.32	719.6	792.9	73.3	1229.1	0.585	50.1	1796.4	2091.8	1.8	4.31×10^{-4}	-0.25
1.76	727.3	795.2	67.9	1234.8	0.589	49.8	1786.2	2049.1	1.4	4.61×10^{-4}	-0.25
2.20	723.3	795.9	72.6	1234.9	0.586	48.6	1673.3	1938.8	1.3	5.42×10^{-4}	-0.25

temperature ($T_{rg}=T_g/T_L$) [65]. Generally, the larger the T_{rg} is, the better the GFA of the alloy is. As shown in Table 1, the T_{rg} is increased when $x \leq 0.44$ at.%, which is similar to the effect of Fe addition on Zr–Cu–Al–(Ni) alloys [57,59] and C addition on $Zr_{52.5}Cu_{17.9}Ni_{14.6}Al_{10}Ti_5$ alloy when the C content is less than 0.1 at.% [63]. However, when x exceeds 0.44 at.%, the T_{rg} is decreased, which is similar to the effect of C addition on $Zr_{41}Ti_{14}Cu_{12.5}Ni_{10}Be_{22.5}$ alloy [62] and the effect of C addition on $Zr_{52.5}Cu_{17.9}Ni_{14.6}Al_{10}Ti_5$ alloy when the C content exceeds 0.1 at.% [63].

Uniaxial compression tests were conducted at a loading rate of $1 \times 10^{-5} \text{ s}^{-1}$ to investigate the mechanical properties of the studied Zr-based BMGs. Figure 3 presents the typical stress–strain curves. It can be readily observed from Fig. 3 that Fe and C additions remarkably enhance both fracture strength and plastic strain. Especially, both fracture strength and plasticity are significantly cooperatively enhanced when x reaches up to 1.32 at.%. In addition, the hardness, yield strength σ_y , fracture strength σ_f , and plastic strain ε_p are carefully identified and tabulated in Table 1. Obviously, Fe and C additions can simultaneously improve the mechanical properties. The hardness improvement in the present work is similar to the effect of C addition on the microhardness of $Zr_{41}Ti_{14}Cu_{12.5}Ni_{10}Be_{22.5}$ BMG [61] and $Zr_{65}Al_{7.5}Ni_{10}Cu_{17.5}$ alloy coatings [63]. The synergistic enhancement of both fracture strength and plasticity are similar to the effect of Fe addition on those of $Zr_{55}Al_{10}Ni_5Cu_{30}$ BMG [58]. The enhancement of the plasticity is also observed in the effect of Fe addition on the plasticity of $Zr_{65}Al_{7.5}Ni_{10}Cu_{17.5}$ BMG [59]. As shown in Table 1, the hardness, σ_y ,

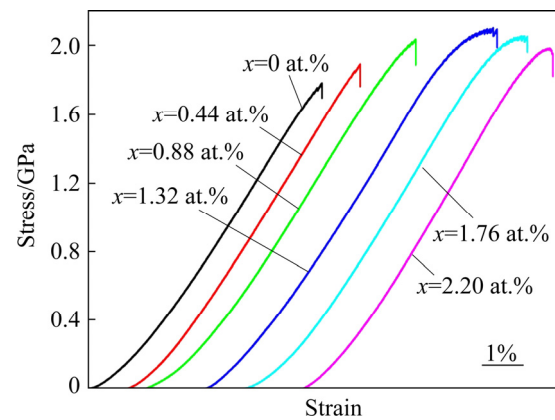


Fig. 3 Compression stress–strain curves of $(Zr_{53}Al_{11.6}Ni_{11.7}Cu_{23.7})_{1-x}(Fe_{77.1}C_{22.9})_x$ ($x=0-2.2$) BMGs at loading rate of $1 \times 10^{-5} \text{ s}^{-1}$ (The curves are horizontally shifted for clarity)

σ_f and ε_p are all increased and then decreased when x reaches up to 1.32 at.%. The dependence of the plasticity on Fe and C content for the studied Zr-based BMGs is similar to that on Fe content for $Zr_{65}Al_{7.5}Ni_{10}Cu_{17.5}$ BMG [59]. Among the studied Zr-based BMGs, the hardness, σ_y , σ_f , and ε_p of the BMG ($x=1.32$ at.%) are all the largest and reach up to HRC 50.1, 1796.4 MPa, 2091.8 MPa, and 1.8%, respectively. The plasticity of the BMG ($x=1.32$ at.%) is six times that of the Fe- and C-free BMG.

To clarify the mechanical behavior of studied Zr-based BMGs, the side and fracture surfaces subjected to the compression tests are examined by SEM. The side views and the fracture morphologies for four typical samples are shown in Fig. 4. As for the Zr-based BMGs ($x \leq 0.44$ at.%) shown in Fig. 4(a), it is clearly found that one shear band parallel to the fracture distributes on the side surface. When x reaches up to 0.88 at.%, as shown in Fig. 4(b), the magnitude of parallel shear bands

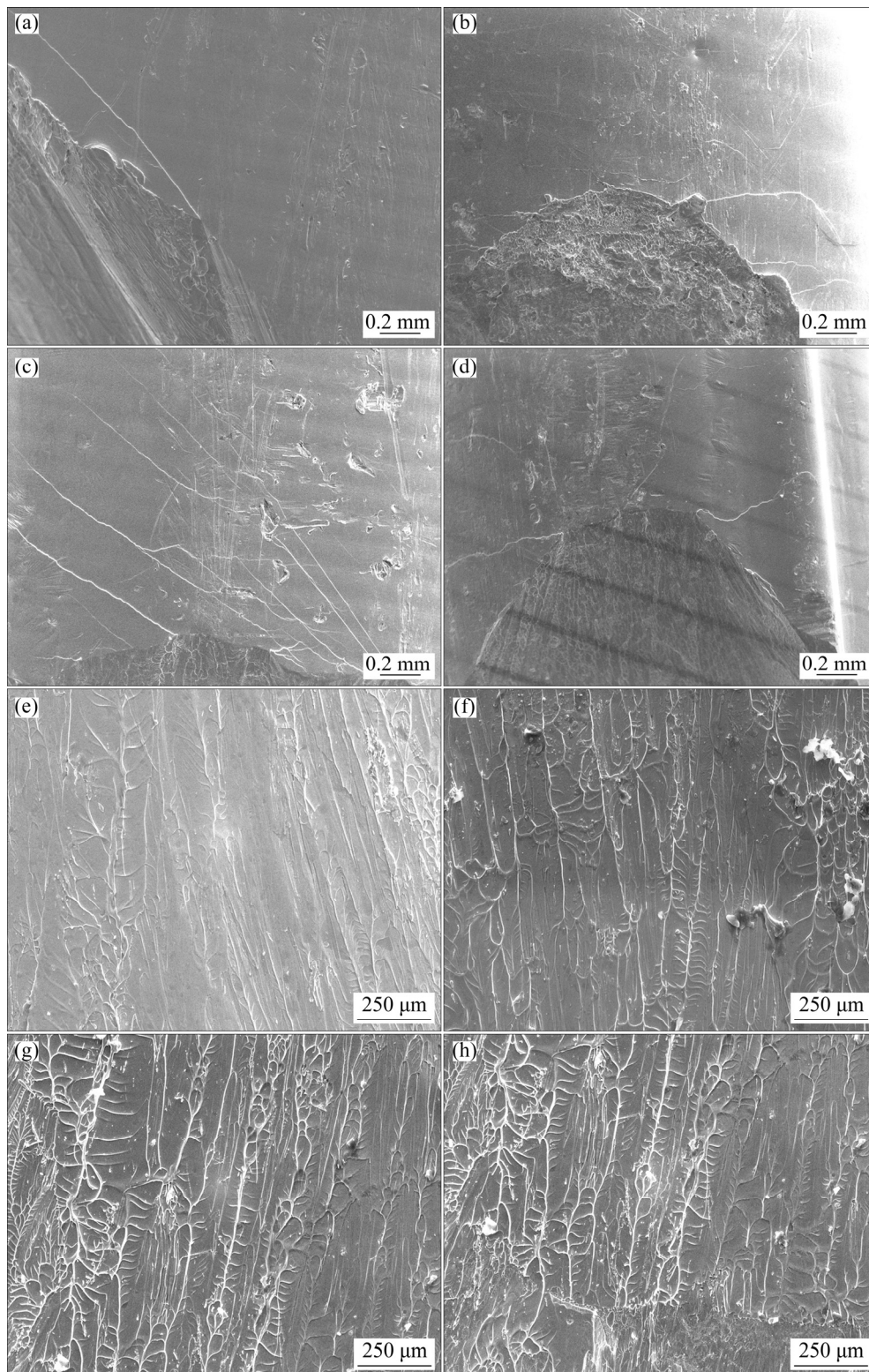


Fig. 4 SEM morphologies of side (a–d) and fracture (e–h) surfaces of $(\text{Zr}_{53}\text{Al}_{11.6}\text{Ni}_{11.7}\text{Cu}_{23.7})_{1-x}(\text{Fe}_{77.1}\text{C}_{22.9})_x$ ($x=0-2.2$) BMGs: (a, e) $x \leq 0.44$; (b, f) $x = 0.88$; (c, g) $x = 1.32$; (d, h) $x \geq 1.76$

significantly increases. The thick shear bands on the right side surface firstly propagate perpendicular to the load and then bend to the fracture. Some fine parallel shear bands on left side surface develop

perpendicular to the direction of the loading. When x increases up to 1.32 at.% (see Fig. 4(c)), large number of shear bands emerge on the side surface and the primary shear bands are parallel to each

other. In addition, the secondary shear bands and the intersection among the shear bands can be readily observed. It is indicated that the propagation of shear bands is effectively hindered during the deformation process, resulting in the high plasticity and strength. As for the Zr-based BMGs ($x \geq 1.76$ at.%) shown in Fig. 4(d), the shear bands are remarkably reduced in the magnitude compared with those for the Zr-based BMG ($x=1.32$ at.%). However, the radial shear bands can be clearly observed on the side surface. On the other hand, the characteristics of vein patterns have been recognized to be related with the plasticity and strength of the MGs. It is generally acknowledged that greater density and smaller size of vein patterns mean comparatively good plasticity and high strength of the MGs. One can see from Figs. 4(e–h) that there are two regions, i.e., vein-like region and smooth region. Compared with Figs. 4(e–g), the area of the smooth regions gradually decreases, while that of the vein patterns gradually increases with increasing x . The vein patterns are gradually well-developed and refined in size, resulting in the increase of the density of the vein patterns. And the vein patterns are finer in Fig. 4(g) than in Fig. 4(h). The density of the vein patterns is higher in Fig. 4(g) than in Fig. 4(h). As a result, the characteristics of the shear bands and vein patterns in Fig. 4 reveal that the propagation of the shear bands is effectively suppressed, which is coherent with the results in Fig. 3 and Table 1.

Electrochemical polarization tests were conducted in 2 wt.% hydrochloric acid solution to evaluate the anti-chloridion corrosion behavior of the studied Zr-based BMGs. The typical polarization curves are shown in Fig. 5. As seen, the anodic current density rapidly increases by slight increase of the potential owing to general corrosion. As the potential increases, a stable current density platform appears. The phenomenon is also observed for other Zr-based BMGs or BMGCs [66,67] in chloride-containing medium. It is indicated that the Zr-based BMGs are in active dissolution or self-passivation state. When the potential increases to a certain value, the current sawteeth appear. Similar phenomena have also been found in Zr–Al–Ni–Nb BMGs corroded in 3% sodium chloride solution [66]. The current sawteeth behavior implies that there are two processes of both pitting and self-passivation. Obviously, the

current sawteeth are remarkably smaller for the Fe- and C-free Zr-based BMG than for the Fe–C micro-alloyed Zr-based BMGs. This means that Fe and C additions lead to the increase of the current sawteeth. It is also indicated that Fe and C additions result in the instability of the passive films of the Zr-based BMGs. In addition, both corrosion current density J_c and corrosion potential ϕ_c are tabulated in Table 1. The ϕ_c is larger for the Fe- and C-free Zr-based BMG than for the Fe–C micro-alloyed Zr-based BMGs, suggesting that Fe and C additions deteriorate the stability of the Zr-based BMGs. The J_c increases with increase of Fe and C content. The J_c is one to two orders of magnitude larger for the Fe–C micro-alloyed Zr-based BMGs than for the Fe- and C-free Zr-based BMG. This implies that Fe and C additions significantly reduce corrosion resistance of the studied Zr-based BMGs.

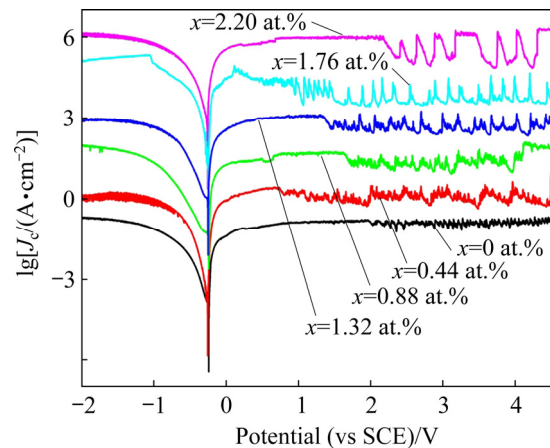


Fig. 5 Polarization curves of $(\text{Zr}_{53}\text{Al}_{11.6}\text{Ni}_{11.7}\text{Cu}_{23.7})_{1-x}(\text{Fe}_{77.1}\text{C}_{22.9})_x$ ($x=0-2.2$) BMGs in 2 wt.% hydrochloric acid solution

In order to further clarify the corrosion behavior and corresponding mechanism, SEM was performed on these BMGs subjected to polarization tests. Figure 6 presents the typical SEM images of the corroded surfaces. As seen from Fig. 6(a), one can only observe the corroded products and no pits on the corroded surface. This suggests that the corrosion mechanism of Fe-free and C-free Zr-based BMG is dominated by the uniform corrosion. When x increases up to 0.44 at.%, some pits and cracked passivating films can be observed on the corrosive surface, as shown in Fig. 6(b), indicating the competition between the pitting and the self-passivation. As x increases up to 0.88 at.%

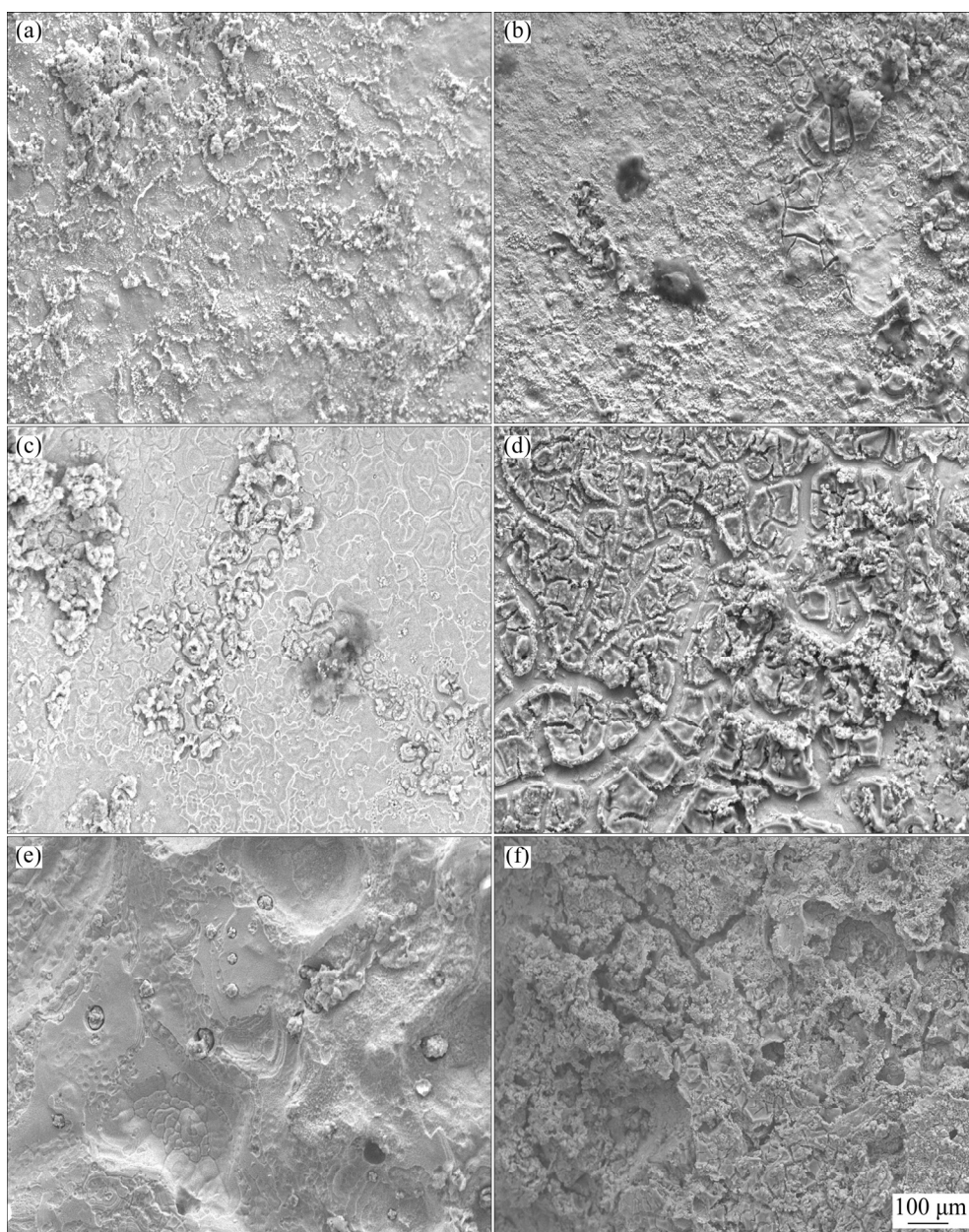


Fig. 6 SEM corrosion micromorphologies of $(\text{Zr}_{53}\text{Al}_{11.6}\text{Ni}_{11.7}\text{Cu}_{23.7})_{1-x}(\text{Fe}_{77.1}\text{C}_{22.9})_x$ ($x=0-2.2$) BMGs: (a) $x=0$; (b) $x=0.44$; (c) $x=0.88$; (d) $x=1.32$; (e) $x=1.76$; (f) $x=2.20$

(Fig. 6(c)), both magnitude and size of the pits increase in comparison with those in Fig. 6(b). Interestingly, the discontinuous passive films are distributed on the corroded surface of the Zr-based BMG ($x=1.32$ at.%), as shown in Fig. 6(d). Nevertheless, the smooth large pits can be clearly observed and predominate for the Zr-based BMG ($x=1.76$ at.%), as shown in Fig. 6(e). When x reaches up to 2.20 at.%, the honeycomb corrosion structure can be clearly seen (see Fig. 6(f)). Therefore, these surface corrosion morphologies reveal that the self-passivation dominates for the Zr-based BMGs ($0 \leq x \leq 0.88$ at.%). The transition

stage from the self-passivation to the pitting corrosion happens when x reaches up to 1.32 at.%. However, the pitting corrosion predominates when x exceeds 1.32 at.%.

4 Discussion

As shown in Table 1, the T_{rg} indicative of the GFA firstly increases and then decreases when x exceeds 0.44 at.%. Inoue's empirical rules state that the multi-component number is beneficial to the formation of amorphous alloy [68]. The Fe and C additions obviously increase the number of the

alloy constitutes, which would improve the GFA of the studied Zr-based BMGs. In addition, large atomic radius difference is also favorable for the formation of amorphous alloy. The atomic radii of Fe and C are the smallest among the alloying elements in the studied Zr-based BMGs, resulting in the enhancement of the GFA. Nevertheless, it has been confirmed that there exists strong covalent bonding between Fe and Al [69], which would lead to the formation of the clusters as the precursors of the crystallization phases. In addition, XU et al [70] found that nanoscale phase separation occurs in the as-prepared $Zr_{48}Cu_{44}Al_7Fe$ BMG when Fe addition was 1–2 at.%. Thus, the GFA of the studied Zr-based glass forming alloys is deteriorated when x exceeds 0.44 at.%. Investigations have revealed that Fe micro-alloying with suitable amount can enhance the GFA of Zr–Ti–Cu–(Ni)–Be alloys [56] and Zr–Al–(Ni)–Cu alloys [57,59]. The GFA of $Zr_{52.5}Cu_{17.9}Ni_{14.6}Al_{10}Ti_5$ alloy [63] was improved when minor addition of C is less than 0.1 at.%, but decreased when C content exceeds 0.1 at.%. On the other hand, both T_g and T_x are increased by Fe and C additions, as shown in Table 1. This indicates that both glass transition and crystallization procedures are retarded by Fe and C additions. It would be related with the microstructure of the BMGs. It has been acknowledged that the glass transition is a process of atomic relaxation and the crystallization requires long-range diffusion of atoms. The Fe and C additions would help to form denser local atomic packing configurations (LAPCs) due to larger atomic mismatch, which would be difficult to cause both atomic relaxation and atomic long-range diffusion. It has been found that appropriate amount of Fe addition can increase the T_x of Zr–Cu–Al alloy [57] and both T_g and T_x of Zr–Al–Ni–Cu alloys [58,59]. In addition, appropriate amount of C addition can increase both T_g and T_x of $Zr_{41}Ti_{14}Cu_{12.5}Ni_{10}Be_{22.5}$ alloy [61].

Figure 3 and Table 1 show that the Fe and C additions simultaneously improve the comprehensive mechanical properties of the studied Zr-based BMGs. It is universally recognized that the deformation of MGs correlates with shear banding which initiates from shear transition zones (STZs). The STZs are considered to be the regions where atoms are easy to be deformed under loading [14,71,72]. The mixing enthalpies of atom pairs are -44 kJ/mol for Al–Zr, -23 kJ/mol for

Zr–Cu, -49 kJ/mol for Zr–Ni, -22 kJ/mol for Al–Ni, -1 kJ/mol for Al–Cu, 4 kJ/mol for Ni–Cu, -25 kJ/mol for Zr–Fe, -11 kJ/mol for Al–Fe, -2 kJ/mol for Fe–Ni, 0 for Ni/Fe/Zr–C, 13 kJ/mol for Fe–Cu, respectively [73]. The negative mixing enthalpy is larger for Fe–Zr pair than for Zr–Cu pair, which would result in the change of local atomic configurations around Zr and Cu atoms [74]. The large positive mixing enthalpy of Fe–Cu pair would stimulate the amorphous phase separation and form Cu-rich region and Fe-rich region [70]. The combination of these effects would even form looser LAPCs around Cu atoms and denser LAPCs around Zr atoms [74]. The small-sized carbon addition would result in forming denser LAPCs as solid solution atoms. In addition, it has been confirmed that there exists strong covalent bonding between Fe and Al, which is advantageous to the formation of the stronger bonded LAPCs [69]. Therefore, the loose LAPCs would provide the fertile regions for the STZs, resulting in the initiation of the shear band. The more densely or strongly bonded LAPCs would impede the propagation of the shear bands. LIU et al [15] found that appropriate proportion of hard region and soft region would synergistically enhance both strength and plasticity of the BMGs. The improvement of the strength and the plasticity by Fe or C addition has been found in Zr-based BMGs [58,59,61,62,70]. For example, the minor addition of Fe significantly enhanced the plasticity of $Zr_{65}Cu_{17.5}Al_{7.5}Ni_{10}$ BMG [59] and $Zr_{48}Cu_{44}Al_8$ BMG [70], and both plasticity and strength of $Zr_{55}Al_{10}Ni_5Cu_{30}$ BMG [58]. C micro-alloying remarkably improved the microhardness of $Zr_{41}Ti_{14}Cu_{12.5}Ni_{10}Be_{22.5}$ BMG [61] and $Zr_{65}Al_{7.5}Ni_{10}Cu_{17.5}$ amorphous composite coatings [63].

As shown in Fig. 5 and Table 1, Fe and C additions significantly influence the corrosion behavior of the studied Zr-based BMGs. The equilibrium electrode potentials are -1.529 V (vs SHE) for Zr/Zr^{4+} , -1.662 V for Al/Al^{3+} , -0.254 V for Ni/Ni^{2+} , -0.037 V for Fe/Fe^{3+} , and 0.337 V for Cu/Cu^{2+} , respectively [75,76]. The large potential difference between Cu and Zr/Al (Ni,Fe) would make preferential dealloying of Zr/Al/Ni/Fe and leave the Cu on the surface, resulting in the initiation of the pits. Meanwhile, the increase of potential leads to the dissolution of Cu left on the surface and then the Cu immediately redeposits into

the pits, resulting in the propagation of the pits [77]. Interestingly, Cu is generally electro-oxidized to porous cuprous chloride complexes in chloride solution [77]. In addition, the cuprous chloride complexes would also combine with chloride ions to form the soluble cuprous chloride complexes. Thus, the pitting is accelerated due to the above-mentioned results. However, Zr, Al and Ni are considered as strong passivating elements and can be easily passivated and form oxide films. Even though Cu can also form oxides, both chemical stability and structural compactness of Zr-, Ti- and Ni-oxides are superior to those of Cu-oxides. The researches have confirmed that the strong passivating elements are usually passivated into uniform dense passivation films, resulting in excellent corrosion property of the BMGs [3,5,27,31,32,37,39,65,66]. Obviously, Fe and C additions reduce the content of strong passive alloying elements such as Zr, Al and Ni in the Fe–C micro-alloyed Zr-based BMGs. EDS results show that Cu enriches in the corroded products/pits, while the strong passive alloying elements such as Zr, Al and Ni enrich in the smooth regions/passive films (not shown in here). Hence, Fe and C additions give rise to the decrease of the ϕ_c and the increase of the J_c in Table 1, and the change of the corrosion microstructure, as shown in Fig. 6.

5 Conclusions

(1) The GFA of the studied Zr-based BMGs is improved when x increases up to 0.44 at.%, and then deteriorated when x exceeds 0.44 at.%. The T_g , T_x , and T_L are all enhanced by Fe and C additions. The T_g and T_x increase by 7–15 K and 1–4 K, respectively. However, the ΔT_x is decreased by 5–11 K.

(2) The hardness, σ_y , σ_f and ε_p are significantly enhanced by the Fe and C additions. The above-mentioned mechanical properties firstly increase and then decrease when x reaches up to 1.32 at.%. The ε_p of the Zr-based BMG ($x=1.32$ at.%) is the largest among the studied Zr-based BMGs and six times that of the Fe-free and C-free Zr-based BMG.

(3) The ϕ_c is slightly decreased by the Fe and C additions. The J_c increases with increase of Fe and C content. The J_c of the Fe–C micro-alloyed Zr-based BMGs is 1–2 orders of magnitude larger

than that of the Fe-free and C-free Zr-based BMG. The pitting corrosion gets more and more serious with increasing Fe and C content. When x rises up to 1.32 at.%, the self-passivation and the pitting corrosion seem well-matched each other.

Acknowledgments

This work was supported by the National Natural Science Foundation of China (No. 51871234), the National Key Research and Development Program of China (No. 2016YFB-0300500), the Open Fund of Key Laboratory of Materials Preparation and Protection for Harsh Environment (Nanjing University of Aeronautics and Astronautics), China, and Ministry of Industry and Information Technology, China (No. XCA19013-04).

References

- [1] INOUE A, TAKEUCHI A. Recent development and application products of bulk glassy alloys [J]. *Acta Materialia*, 2011, 59: 2243–2267.
- [2] WU Hong, BAKER Ian, LIU Yong, WU Xiao-lan. Dry sliding tribological behavior of Zr-based bulk metallic glass [J]. *Transactions of Nonferrous Metals Society of China*, 2012, 22: 585–589.
- [3] KHAN M M, SHABIB I, HAIDER W. A combinatorially developed Zr–Ti–Fe–Al metallic glass with outstanding corrosion resistance for implantable medical devices [J]. *Scripta Materialia*, 2019, 162: 223–229.
- [4] JABED A, KHAN M M, CAMILLER J, WACKER M G, HAIDER W, SHABIB I. Property optimization of Zr–Ti–X (X=Ag, Al) metallic glass via combinatorial development aimed at prospective biomedical application [J]. *Surface Coating Technology*, 2019, 372: 278–287.
- [5] LI J, SHI L L, ZHU Z D, HE Q, AI H J, XU J. Zr₆₁Ti₂Cu₂₅Al₁₂ metallic glass for potential use in dental implants: Biocompatibility assessment by in vitro cellular responses [J]. *Materials Science and Engineering C*, 2013, 33: 2113–2121.
- [6] LIU Y, WANG Y M, PANG H F, ZHAO Q, LIU L. A Ni-free ZrCuFeAlAg bulk metallic glass with potential for biomedical applications [J]. *Acta Biomaterialia*, 2013, 9: 7043–7053.
- [7] LIU Z Q, HUANG L, WU W, LUO X K, SHI M J, LIAW P K, HE W, ZHANG T. Novel low Cu content and Ni-free Zr-based bulk metallic glasses for biomedical applications [J]. *Journal of Non-Crystalline Solids*, 2013, 363: 1–5.
- [8] HUA N B, HUANG L, HE W, PANG S J, ZHANG T. A Ni-free high-zirconium-based bulk metallic glass with enhanced plasticity and biocompatibility [J]. *Journal of Non-Crystalline Solids*, 2013, 376: 133–138.
- [9] BOUALA G I N, ETIEMBLE A, LOUGHIAN C D, LANGLOIS C, PIERSON J F, STEYER P. Silver influence

- on the antibacterial activity of multi-functional Zr–Cu based thin film metallic glasses [J]. *Surface Coating Technology*, 2018, 343: 108–114.
- [10] LEE J, LIOU M L, DUH J G. The development of a Zr–Cu–Al–Ag–N thin film metallic glass coating in pursuit of improved mechanical, corrosion, and antimicrobial property for bio-medical application [J]. *Surface Coating Technology*, 2017, 310: 214–222.
- [11] CHEN H W, HSU K C, CHAN Y C, DUH J G, LEE J W, JANG J S C, CHEN G J. Antimicrobial properties of Zr–Cu–Al–Ag thin film metallic glass [J]. *Thin Solid Films*, 2014, 561: 98–101.
- [12] CHU J H, LEE J, CHANG C C, CHAN Y C, LIOU M L, LEE J W, JANG J S C, DUH J G. Antimicrobial characteristics in Cu-containing Zr-based thin film metallic glass [J]. *Surface Coating Technology*, 2014, 259: 87–93.
- [13] ZONG H T, GENG C C, KANG C Y, CAO G H, LI L X, ZHANG B Q, LI M. Excellent near-infrared transmission of Zr-based thin film metallic glasses [J]. *Results in Physics*, 2018, 10: 612–615.
- [14] KASSA S T, HU C C, LIAO Y C, CHEN J K, CHU J P. Thin film metallic glass as an effective coating for enhancing oil/water separation of electrospun polyacrylonitrile membrane [J]. *Surface Coating Technology*, 2019, 368: 33–41.
- [15] LIU Y H, WANG G, WANG R J, ZHAO D Q, PAN M X, WANG W H. Super plastic bulk metallic glasses at room temperature [J]. *Science*, 2017, 315: 1385–1388.
- [16] YOKOYAMA Y, FUJITAB K, YAVARI A R, INOUE A. Malleable hypoeutectic Zr–Ni–Cu–Al bulk glassy alloys with tensile plastic elongation at room temperature [J]. *Philosophical Magazine Letter*, 2009, 89: 322–324.
- [17] WU Hong, LIU Yong, LI Kai-yang, ZHAO Zhong-wei. Casting effect on compressive brittleness of bulk metallic glass [J]. *Transactions of Nonferrous Metals Society of China*, 2014, 24: 385–392.
- [18] WU FF, JIANG S S, ZHAO R D, ZHOU Q, ZHANG G A, WU X F. Size-dependent plastic stability of Zr-based metallic glass [J]. *Materials Science and Engineering A*, 2015, 646: 272–278.
- [19] ZHOU X L, ZHOU H F, LI X Y, CHEN C Q. Size effects on tensile and compressive strengths in metallic glass nanowires [J]. *Journal of the Mechanics and Physics of Solids*, 2015, 84: 130–144.
- [20] YANG Y J, CHENG B Y, LV J W, LI B, MA M Z, ZHANG X Y, LI G, LIU R P. Effect of Ag substitution for Ti on glass-forming ability, thermal stability and mechanical properties of Zr-based bulk metallic glasses [J]. *Materials Science and Engineering A*, 2019, 746: 229–238.
- [21] RAHVARD M M, TAMIZIFAR M, BOUTORABI S M A. The effect of Ag addition on the non-isothermal crystallization kinetics and fragility of $Zr_{56}Co_{28}Al_{16}$ bulk metallic glass [J]. *Journal of Non-Crystalline Solids*, 2018, 481: 74–84.
- [22] ZHOU W, HOU J X, ZHONG Z Z, LI J F. Effect of Ag content on thermal stability and crystallization behavior of Zr–Cu–Ni–Al–Ag bulk metallic glass [J]. *Journal of Non-Crystalline Solids*, 2015, 411: 132–136.
- [23] CUI X, ZU F Q, JIANG W X, WANG L F, WANG Z Z. Achieving superior glass forming ability of Zr–Cu–Al–Ni–Ti/Ag bulk metallic glasses by element substitution [J]. *Journal of Non-Crystalline Solids*, 2013, 375: 83–87.
- [24] GUO W, SHAO Y M, SAIDA J, ZHAO M, LÜ S L, WU S S. Rejuvenation and plasticization of Zr-based bulk metallic glass with various Ta content upon deep cryogenic cycling [J]. *Journal of Alloys and Compounds*, 2019, 795: 314–318.
- [25] LI T H, LIAO Y C, SONG S M, JIANG Y L, TSAI P H, JANG J S C, HUANG J C. Significantly enhanced mechanical properties of ZrAlCo bulk amorphous alloy by microalloying with Ta [J]. *Intermetallics*, 2018, 93: 162–168.
- [26] CAO G H, LIU K, LIU G P, ZONG H T, BALA H, ZHANG B Q. Improving the glass-forming ability and the plasticity of Zr–Cu–Al bulk metallic glass by addition of Nb [J]. *Journal of Non-Crystalline Solids*, 2019, 513: 105–110.
- [27] CAO Q P, PENG S, ZHAO X N, WANG X D, ZHANG D X, JIANG J Z. Effect of Nb substitution for Cu on glass formation and corrosion behavior of ZrCuAgAlBe bulk metallic glass [J]. *Journal of Alloys and Compounds*, 2016, 683: 22–31.
- [28] CHEN S S, TODD I. Enhanced plasticity in the Zr–Cu–Ni–Al–Nb alloy system by in-situ formation of two glassy phases [J]. *Journal of Alloys and Compounds*, 2015, 646: 973–977.
- [29] JIN Z S, YANG Y J, ZHANG Z P, MA X Z, LV J W, WANG F L, MA M Z, ZHANG X Y, LIU R P. Effect of Hf substitution Cu on glass-forming ability, mechanical properties and corrosion resistance of Ni-free Zr–Ti–Cu–Al bulk metallic glasses [J]. *Journal of Alloys and Compounds*, 2019, 806: 668–675.
- [30] ZHANG Y, YAO J, ZHAO X Y, MA L Q. Ti substituted Ni-free $Zr_{65-x}Ti_xCu_{17.5}Fe_{10}Al_{7.5}$ bulk metallic glasses with significantly enhanced glass-forming ability and mechanical properties [J]. *Journal of Alloys and Compounds*, 2019, 773: 713–718.
- [31] SHI H Q, ZHAO W B, WEI X W, DING Y, SHEN X D, LIU W J. Effect of Ti addition on mechanical properties and corrosion resistance of Ni-free Zr-based bulk metallic glasses for potential biomedical applications [J]. *Journal of Alloys and Compounds*, 2020, 815: 152636.
- [32] ZHUANG Yan-xin, WANG Shen-ci, WANG Chang-jiu, WANG Nai-peng, HE Ji-cheng. Effect of Ti on microstructure, mechanical and corrosion properties of $(Zr_{0.55}Al_{0.1}Ni_{0.05}Cu_{0.3})_{100-x}Ti_x$ bulk metallic glasses [J]. *Transactions of Nonferrous Metals Society of China*, 2016, 26: 138–143.
- [33] SHI B, XU Y L, MA W L, LI C, ESTEFANIA C V, LI J G. Effect of Ti addition on the glass forming ability, crystallization, and plasticity of $(Zr_{64.13}Cu_{15.75}Ni_{10.12}Al_{10})_{100-x}Ti_x$ bulk metallic glasses [J]. *Materials Science and Engineering A*, 2015, 639: 345–349.
- [34] LI P, WANG J J, CHENG J L, LI F, ZHAO W, CHEN G. Investigation of the effects of Al on the glass forming ability of Zr–Cu–Ni–Al alloys through their solidification characteristics [J]. *Intermetallics*, 2019, 109: 105–109.
- [35] ZÍTEK M, ZEMAN P, KOTRLOVÁ M, ČERSTVÝ R. Impact of Al or Si addition on properties and oxidation resistance of magnetron sputtered Zr–Hf–Al/Si–Cu metallic glasses [J]. *Journal of Alloys and Compounds*, 2019, 772:

- 409–417.
- [36] LU S D, SUN S C, LI K H, LI H Y, HUANG X X, TU G F. The effect of Y addition on the crystallization behaviors of Zr–Cu–Ni–Al bulk metallic glasses [J]. *Journal of Alloys and Compounds*, 2019, 799: 501–512.
- [37] YU L S, TANG J L, WANG H, WANG Y Y, QIAO J C, APREUTESEI M, NORMAND B. Corrosion behavior of bulk $(\text{Zr}_{58}\text{Nb}_3\text{Cu}_{16}\text{Ni}_{13}\text{Al}_{10})_{100-x}\text{Y}_x$ ($x=0, 0.5, 2.5$ at.%) metallic glasses in sulfuric acid [J]. *Corrosion Science*, 2019, 150: 42–53.
- [38] ZHU J H, WANG C P, HAN J J, YANG S Y, XIE G Q, JIANG H X, CHEN Y C, LIU X J. Formation of Zr-based bulk metallic glass with large amount of yttrium addition [J]. *Intermetallics*, 2018, 92: 55–61.
- [39] LU S D, SUN S C, TU G F, HUANG X X, LI K H. The effect of yttrium addition on the air oxidation behavior of Zr–Cu–Ni–Al bulk metallic glasses at 400–500 °C [J]. *Corrosion Science*, 2018, 137: 53–61.
- [40] ZHOU K, LIU Y, PANG S J, ZHANG T. Formation and properties of centimeter-size Zr–Ti–Cu–Al–Y bulk metallic glasses as potential biomaterials [J]. *Journal of Alloys and Compounds*, 2016, 656: 389–394.
- [41] ZHANG Y, YAN L, ZHAO X Y, MA L Q. Enhanced chloride ion corrosion resistance of Zr-based bulk metallic glasses with cobalt substitution [J]. *Journal of Non-Crystalline Solids*, 2018, 496: 18–23.
- [42] WANG T, SI J J, WU Y D, LV K, LIU Y H, HHUI X D. Two-step work-hardening and its gigantic toughening effect in Zr-based bulk metallic glasses [J]. *Scripta Materialia*, 2018, 150: 106–109.
- [43] ZHANG Y, ZHOU M, ZHAO X Y, MA L Q. Co substituted Zr–Cu–Al–Ni metallic glasses with enhanced glass-forming ability and high plasticity [J]. *Journal of Non-Crystalline Solids*, 2017, 473: 120–124.
- [44] DONG Y, WUNDERLICH R, BISKUPEK J, CAO Q P, WANG X D, ZHANG D X, JIANG J Z, FECHT H J. Co content effect on elastic strain limit in ZrCuNiAlCo bulk metallic glasses [J]. *Scripta Materialia*, 2017, 137: 94–99.
- [45] HAN K M, QIANG J B, WANG Y M, HÄUSSLER P. Zr–Al–Co–Cu bulk metallic glasses for biomedical devices applications [J]. *Journal of Alloys and Compounds*, 2017, 729: 144–149.
- [46] ZHOU W, WENG W P, HOU J X. Glass-forming ability and corrosion resistance of ZrCuAlCo bulk metallic glass [J]. *Journal of Materials Science and Technology*, 2016, 32: 349–354.
- [47] ZHOU K, CHEN C, LIU Y, PANG S J, HUA N B, YANG W, ZHANG T. Effects of lutetium addition on formation, oxidation and tribological properties of a Zr-based bulk metallic glass [J]. *Intermetallics*, 2017, 90: 81–89.
- [48] HUA N B, CHEN W Z. Enhancement of glass-forming ability and mechanical property of Zr-based Zr–Al–Ni bulk metallic glasses with addition of Pd [J]. *Journal of Alloys and Compounds*, 2017, 693: 816–824.
- [49] ZHOU W, HOU J X, WENG W P. Microstructure, thermal stability and mechanical properties of Zr–Cu–Al–Sn bulk metallic glass [J]. *Journal of Non-Crystalline Solids*, 2015, 429: 208–212.
- [50] WANG P C, LEE J W, YANG Y C, LOU B S. Effects of silicon contents on the characteristics of Zr–Ti–Si–W thin film metallic glasses [J]. *Thin Solid Films: Part A*, 2016, 618: 28–35.
- [51] CHANG Y S, HSU K T, LI J B, TSAI P H, JANG J S C, HUANG J C. Effect of cast process and microalloying on the fracture toughness of Zr-based bulk amorphous alloys [J]. *Journal of Alloys and Compounds*, 2014, 614: 87–93.
- [52] XU J, ZHAO Z F, ZUO M, XING Q, SUN Z X, WANG Y. Effects of Ca addition on the glass formation, microhardness and corrosion resistance in different solutions of $\text{Zr}_{66.7-x}\text{Ni}_{33.3}\text{Ca}_x$ ($x=0, 1, 3$ and 5 at.%) metallic glasses [J]. *Journal of Alloys and Compounds*, 2014, 595: 178–184.
- [53] KHADEMIAN N, GHOLAMIPOUR R, SHAHRI F, TAMIZIFAR M. Effect of vanadium substitution for zirconium on the glass forming ability and mechanical properties of a $\text{Zr}_{65}\text{Cu}_{17.5}\text{Ni}_{10}\text{Al}_{7.5}$ bulk metallic glass [J]. *Journal of Alloys and Compounds*, 2013, 546: 41–47.
- [54] MOHAMMADI RAHVARD M, TAMIZIFAR M, BOUTORABI S M A. Zr–Co(Cu)–Al bulk metallic glasses with optimal glass-forming ability and their compressive properties [J]. *Transactions of Nonferrous Metals Society of China*, 2018, 28: 1543–1552.
- [55] ZHAO D Q, ZHANG Y, PAN M X, WANG W H. The effects of iron addition on the glass forming ability and properties of Zr–Ti–Ni–Cu–Be–Fe bulk metallic glass [J]. *Materials Transactions JIM*, 2000, 41: 1427–1431.
- [56] ZONG H T, BIAN L Y, CHENG J Y, CAO G H, KANG C Y, LI M. Glass forming ability, thermal stability and elastic properties of Zr–Ti–Cu–Be–(Fe) bulk metallic glasses [J]. *Results in Physics*, 2016, 6: 1157–1160.
- [57] ZHANG Q S, ZHANG W, INOUE A. Ni-free Zr–Fe–Al–Cu bulk metallic glasses with high glass-forming ability [J]. *Scripta Materialia*, 2009, 61: 241–244.
- [58] LIU Guang-qiao, KOU Sheng-zhong, LI Chun-yan, ZHAO Yan-chun, SUO Hong-li. Effect of minor Fe addition on glass forming ability and mechanical properties of $\text{Zr}_{55}\text{Al}_{10}\text{Ni}_5\text{Cu}_{30}$ bulk metallic glass [J]. *Transactions of Nonferrous Metals Society of China*, 2012, 22: 590–595.
- [59] ZHOU M, ZHOU J X, WEI J, YANG M, MA L Q. Enhanced glass-forming ability and mechanical properties of $\text{Zr}_{65}\text{Cu}_{17.5}\text{Al}_{7.5}\text{Ni}_{10}$ metallic glass by adding Fe [J]. *Journal of Non-Crystalline Solids*, 2017, 455: 1–5.
- [60] QIAO J C, CONG J, WANG Q, PELLETIER J M, YAO Y. Effects of iron addition on the dynamic mechanical relaxation of $\text{Zr}_{55}\text{Cu}_{30}\text{Ni}_5\text{Al}_{10}$ bulk metallic glasses [J]. *Journal of Alloys and Compounds*, 2018, 749: 262–267.
- [61] WANG W H, WEI Q, BAI H Y. Enhanced thermal stability and microhardness in Zr–Ti–Cu–Ni–Be bulk amorphous alloy by carbon addition [J]. *Applied Physics Letter*, 1997, 71: 58–60.
- [62] ZHANG Y, ZHAO D Q, PAN M X, WANG W H. Glass forming properties of Zr-based bulk metallic alloys [J]. *Journal of Non-Crystalline Solids*, 2003, 315: 206–210.
- [63] KÜNDIG A A, LEPORI D, PERRY A J, ROSSMANN S, BLATTER A, DOMMANN A, UGGOWITZER P J. Influence of low oxygen contents and alloy refinement on the glass forming ability of $\text{Zr}_{52.5}\text{Cu}_{17.9}\text{Ni}_{14.6}\text{Al}_{10}\text{Ti}_5$ [J]. *Materials Transactions*, 2002, 43: 3206–3210.

- [64] WANG Y F, LI G, SHI Z Q, LIU M X, ZHANG X Y, LIU Y. Effects of graphite addition on the microstructure and properties of laser cladding Zr–Al–Ni–Cu amorphous coatings [J]. *Journal of Alloys and Compounds*, 2014, 610: 713–717.
- [65] TURNBULL D. Under what conditions can a glass be formed? [J]. *Contemporary Physics*, 1969, 10(5): 473–488.
- [66] LI Y H, ZHANG W, DONG C, QIN C L, QIANG J B, MAKINO A, INOUE A. Enhancement of glass-forming ability and corrosion resistance of Zr-based Zr–Ni–Al bulk metallic glasses with minor addition of Nb [J]. *Journal of Applied Physics*, 2011, 110: 023513.
- [67] LIU L, QIU C L, ZOU H, CHAN K C. The effect of the microalloying of Hf on the corrosion behavior of ZrCuNiAl bulk metallic glass [J]. *Journal of Alloys and Compounds*, 2005, 399: 144–148.
- [68] INOUE A. High strength bulk amorphous alloys with low critical cooling rates [J]. *Materials Transactions JIM*, 1995, 36: 866–875.
- [69] ZHANG B, WANG R J, ZHAO D Q, PAN M X, WANG W H. Superior glass-forming ability through microalloying in cerium-based alloys [J]. *Physical Review B*, 2006, 73: 092201.
- [70] XU H W, DU Y L, DENG Y. Effect of minor-addition of Fe on structural and mechanical properties of CuZrAl bulk metallic glass [J]. *Transactions of Nonferrous Metals Society of China*, 2012, 22: 1123–1126.
- [71] WANG W H. The elastic properties, elastic models and elastic perspectives of metallic glasses [J]. *Progressive Materials Science*, 2012, 57: 487–656.
- [72] MA E. Tuning order in disorder [J]. *Nature Materials*, 2015, 14: 547–552.
- [73] TAKEUCHI A, INOUE A. Calculation of mixing enthalpy and mismatch entropy for ternary amorphous alloys [J]. *Materials Transactions JIM*, 2000, 41: 1372–1378.
- [74] GUO G Q, YANG L, WU S Y. Structural investigation upon the high glass-forming ability in Fe-doped ZrCuAl multicomponent alloys [J]. *Intermetallics*, 2016, 71: 24–30.
- [75] CAI A H, TAN J, DING D W, WANG H, LIU Y, WU H, AN Q, NING H, ZHOU G J. Effect of Al addition on properties of Cu₄₅Zr_{45.5}Ti_{9.5} bulk metallic glass [J]. *Materials Chemistry and Physics*, 2020, 251: 123072.
- [76] CAI A H, FENG Y J, DING D W, LIU Y, WU H, AN Q, NING H, ZHOU G J. PENG Y Y. Effect of Fe–C alloy additions on properties of Cu–Zr–Ti metallic glasses [J]. *Journal of Alloys and Compounds*, 2019, 798: 273–279.
- [77] LU H B, ZHANG L C, GEBERT A, SCHULTZ L. Pitting corrosion of Cu–Zr metallic glasses in hydrochloric acid solutions [J]. *Journal of Alloys and Compounds*, 2008, 462: 60–67.

Fe–C 微合金化对 $Zr_{53}Al_{11.6}Ni_{11.7}Cu_{23.7}$ 块体金属玻璃性能的影响

丁大伟^{1,2}, 谭靖³, 蔡安辉³, 刘咏⁴, 吴宏⁴, 安琪³, 李鹏伟³, 张焱³, 阳清³

1. 中国科学院 物理研究所, 北京 100190;
2. 松山湖材料实验室, 东莞 523808;
3. 湖南理工学院 机械工程学院, 岳阳 414000;
4. 中南大学 粉末冶金国家重点实验室, 长沙 410083

摘要: 采用水冷铜模吸铸法制备 $(Zr_{53}Al_{11.6}Ni_{11.7}Cu_{23.7})_{1-x}(Fe_{77.1}C_{22.9})_x$ ($x=0\sim 2.2$, 摩尔分数, %) 块体金属玻璃, 系统研究其玻璃形成能力和物理化学性能。结果表明, 随着 x 的增大, 玻璃形成能力得到提高, 但当 x 大于 0.44% 时, 玻璃形成能力降低; Fe–C 的添加使玻璃转变温度和晶化温度同时升高, 但使过冷液相区变窄。块体金属玻璃的硬度、屈服和断裂强度以及塑性首先随 Fe–C 含量的增加而增加, 但当 x 增加到 1.32% 时, 这些性能下降; 含 1.32% Fe–C 的块体金属玻璃的塑性应变是不含 Fe 和 C 的块体金属玻璃的 6 倍。Fe–C 微合金化后, 块体金属玻璃的腐蚀电位轻微下降, 然而腐蚀电流密度增加; 随着 Fe–C 合金含量的增加, 点蚀变得越来越严重。

关键词: 锆基金属玻璃; 腐蚀性能; 热学性能; 力学性能; Fe–C 微合金化

(Edited by Bing YANG)